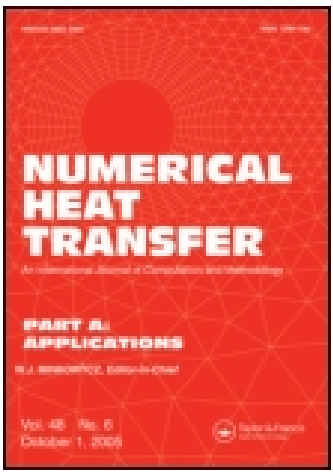

Numerical Heat Transfer, Part A: Applications: An International Journal of Computation and Methodology

Publication details, including instructions for authors and subscription information:
http://www.tandfonline.com/loi/unht20

NATURAL CONVECTION IN A 2D ENCLOSURE WITH SINUSOIDAL UPPER WALL TEMPERATURE

I. E. Sarris , I. Lekakis & N. S. Vlachos

Published online: 30 Nov 2010.

To cite this article: I. E. Sarris , I. Lekakis & N. S. Vlachos (2002) NATURAL CONVECTION IN A 2D ENCLOSURE WITH SINUSOIDAL UPPER WALL TEMPERATURE, Numerical Heat Transfer, Part A: Applications: An International Journal of Computation and Methodology, 42:5, 513-530, DOI: 10.1080/10407780290059675

To link to this article: http://dx.doi.org/10.1080/10407780290059675

Numerical Heat Transfer, Part A, 42: 513–530, 2002

1040-7782/02 $12.00 + .00
DOI: 10.1080/1040778029005967 5

NATURAL CONVECTION IN A 2D ENCLOSURE WITH SINUSOIDAL UPPER WALL TEMPERATURE

I. E. Sarris, I. Lekakis, and N. S. Vlachos

Laboratory of Fluid Mechanics and Turbomachinery, Department of Mechanical and Industrial Engineering, University of Thessaly, Volos, Greece

Natural convection in a two-dimensional, rectangular enclosure with sinusoidal temperature profile on the upper wall and adiabatic conditions on the bottom and sidewalls is numerically investigated. The applied sinusoidal temperature is symmetric with respect to the midplane of the enclosure. Numerical calculations are produced for Rayleigh numbers in the range 10^2 to 10^8, and results are presented in the form of streamlines, isotherm contours, and distributions of local Nusselt number. The circulation patterns are shown to increase in intensity, and their centers to move toward the upper wall corners with increasing Rayleigh number. As a result, the thermal boundary layer is confined near the upper wall regions. The values of the maximum and the minimum local Nusselt number at the upper wall are shown to increase with increasing Rayleigh number. Finally, an increase in the enclosure aspect ratio produces an analogous increase of the fluid circulation intensity.

INTRODUCTION

Natural convection in fluid-filled rectangular enclosures has received considerable attention in recent years because of its relation to the thermal performance of many engineering installations. This work was motivated by the need to understand the heat transfer characteristics in glass melting tanks, where a number of burners placed above the glass tank create periodic temperature profiles on the surface of the glass melt; see Sarris et al. [1] and Jian et al. [2].

The studies of natural convection in fluid-filled cavities primarily have been concentrated on cases of heating from the bottom wall or sidewalls; see Ostrach [3]. A limited amount of work has been reported on the more complex case of cooling from the top wall, mainly with simultaneous heating of a sidewall; see Aydin et al. [4]. There exist several studies in the literature on the natural convection with periodic temperature conditions imposed upon the bottom or sidewalls. For example, Poulikakos [5] studied an enclosure with its left sidewall differentially heated, one

Received 10 May 2001; accepted 31 January 2002.

This work was partially funded by the General Secretariat for Research and Technology (contract EPET-II/296). The leading author is grateful to the Research Board of the University of Thessaly for a research grant (EE 2418). The authors also thank Mr. N. Katsavos for his help.

Address correspondence to Dr. N. S. Vlachos, Department of Mechanical and Industrial Engineering, University of Thessaly, Athens Avenue, 38334 Volos, Greece. E-mail: vlachos@mie.uth.gr

NOMENCLATURE

g	gravitational acceleration	α	thermal diffusivity
H	height of the enclosure	β	coefficient of thermal expansion
L	length of the enclosure	δ_t	thickness of the thermal boundary layer
Nu	Nusselt number	Θ	nondimensional temperature
p	pressure of the fluid	ν	fluid kinematic viscosity
P	dimensionless pressure	ρ	fluid density
Pr	Prandtl number	φ	generalized variable
Ra	Rayleigh number	ψ	stream function
T	fluid temperature	Ψ	nondimensional stream function
$T_w(x)$	upper wall temperature distribution	**Subscripts**	
u, v	velocity components in x- and y-directions	c	cold
U, V	dimensionless velocity components	h	hot
x, y	spatial coordinates	i, j	coordinate indices
X, Y	dimensionless coordinates	mp	middle plane
		t	thermal

half of the wall is heated and the other half is cooled, and the remaining walls are insulated. He showed that a penetrating thermal layer is formed, the size of which is a function of Rayleigh number and aspect ratio of the enclosure. Bilgen et al. [6] used a system of discrete temperature sources placed periodically on the bottom wall of a shallow cavity. Lakhal et al. [7] also studied transient natural convection heat transfer in a square enclosure with part of the bottom wall under uniform time-varying temperature conditions. Lage and Bejan [8] studied enclosures with one sidewall heated using a pulsating heat flux and the other sidewall cooled at constant temperature. They showed that at high Rayleigh numbers, the buoyancy driven flow has the tendency to resonate to the periodic heating that has been supplied from the side.

Uniform heating on the top wall of an enclosure results in flow stratification, but nonuniform heating produces counter-rotating circulation patterns. Studies of natural convection in molten glass cells with periodic heating from above and specified temperature on the sidewalls for Rayleigh numbers up to 10^7 were made by Wright and Rawson [9] and Burley et al. [10]. Periodic heating from above has strong implications for the glass industry, where the main objective is to increase the mixing of the glass melt.

In this study, natural convection in enclosures with periodic heating from above over the entire top wall and adiabatic bottom and sidewall boundary conditions is studied for the first time as it appears in the literature. Periodic heating from the upper wall is expected to produce a pair of well-defined circulation patterns, while adiabatic conditions on the other boundaries ensure that only the upper wall heating controls the flow. The effect of Rayleigh number on the flow patterns and the resulting heat transfer is determined. In addition the effect of the enclosure aspect ratio is studied for the value of Rayleigh numbers from 10^3 to 10^8.

PROBLEM SPECIFICATION

A two-dimensional rectangular enclosure completely filled with a viscous fluid is considered, as shown in Figure 1. The side and bottom walls are assumed to be

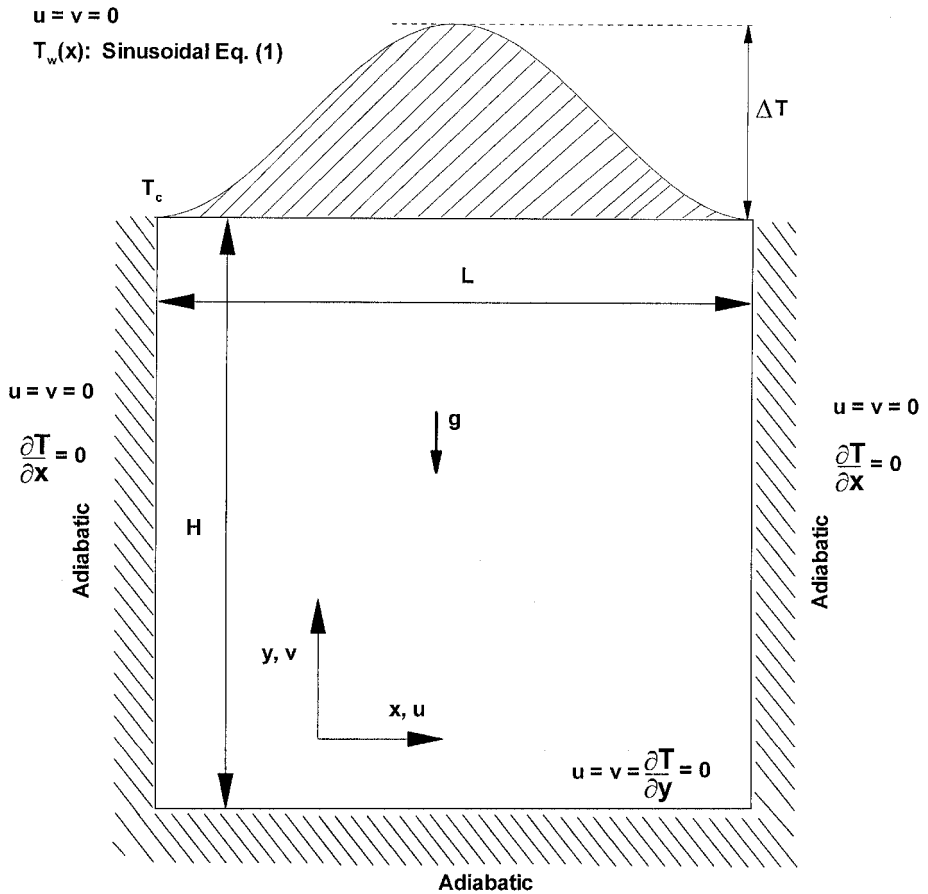

Figure 1. Flow configuration and boundary conditions.

adiabatic while a sinusoidal temperature distribution $T_w(x)$ is applied on the top wall as follows:

$$T_w(x) = T_c + \frac{\Delta T}{2}\left(1 - \cos\left(\frac{2\pi x}{L}\right)\right) \tag{1}$$

where T_c is the minimum value of the imposed temperature distribution, ΔT is the temperature difference between the maximum and the minimum temperatures of the upper wall, and L is the length of the enclosure.

MATHEMATICAL FORMULATION

The present flow is considered laminar and two dimensional, while the usual Boussinesq approximation for treatment of the buoyant term in the momentum

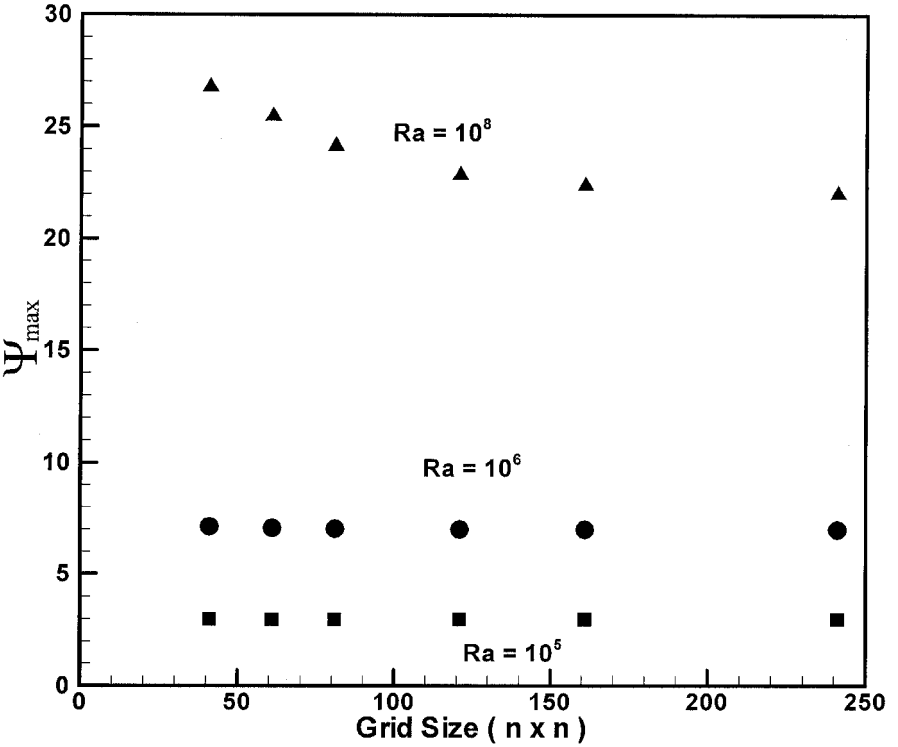

Figure 2. Variation of Ψ_{max} with grid size for $Ra = 10^5$, 10^6, and 10^8.

equation is adopted. The governing equations and the boundary conditions are cast in dimensionless form using the following dimensionless variables:

$$X = \frac{x}{H} \quad Y = \frac{y}{H} \quad U = \frac{uH}{\alpha} \quad V = \frac{vH}{\alpha} \tag{2}$$

$$P = \frac{pH^2}{\rho\alpha^2} \qquad \Theta = \frac{T - T_c}{\Delta T} \tag{3}$$

where P and Θ are the nondimensional pressure and temperature, respectively, and U and V are the nondimensional velocity components in the x- and y-directions, respectively.

With the above-defined variables the governing equations become

Continuity

$$\frac{\partial U}{\partial X} + \frac{\partial V}{\partial Y} = 0 \tag{4}$$

X-momentum

$$U\frac{\partial U}{\partial X} + V\frac{\partial U}{\partial Y} = -\frac{\partial P}{\partial X} + \mathrm{Pr}\nabla^2 U \tag{5}$$

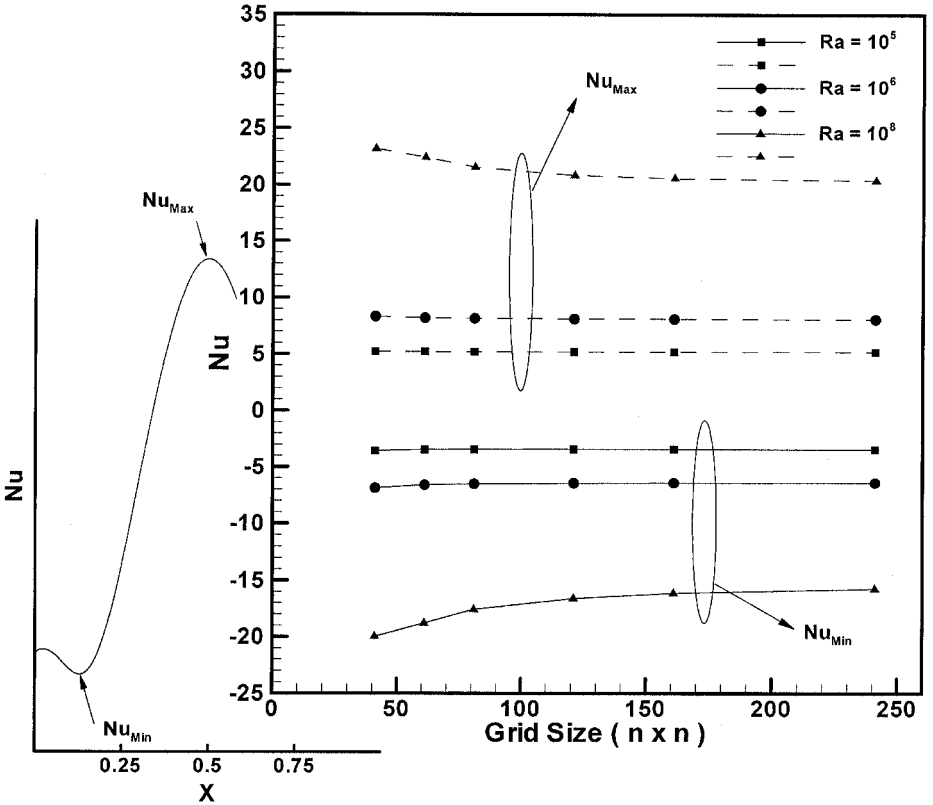

Figure 3. Effect of grid size on the maximum and minimum Nu at the top wall for $Ra = 10^5$, 10^6, and 10^8.

Y-momentum

$$U\frac{\partial V}{\partial X} + V\frac{\partial V}{\partial Y} = -\frac{\partial P}{\partial Y} + \mathrm{Pr}\nabla^2 V + \mathrm{Ra}\,\mathrm{Pr}\Theta \tag{6}$$

Energy

$$U\frac{\partial \Theta}{\partial X} + V\frac{\partial \Theta}{\partial Y} = \nabla^2 \Theta \tag{7}$$

where $\mathrm{Pr} = \nu/\alpha$ and $\mathrm{Ra} = g\beta\Delta T H^3/\nu\alpha$ are the Prandtl and Rayleigh numbers, respectively.

In addition, the velocity and temperature boundary conditions, take the following form:

$$\left.\begin{array}{l} U = V = 0 \\ \frac{\partial \Theta}{\partial X} = 0 \end{array}\right\} \quad \text{for} \quad X = 0, 1 \text{ and } 0 \le Y \le 1 \tag{8a}$$

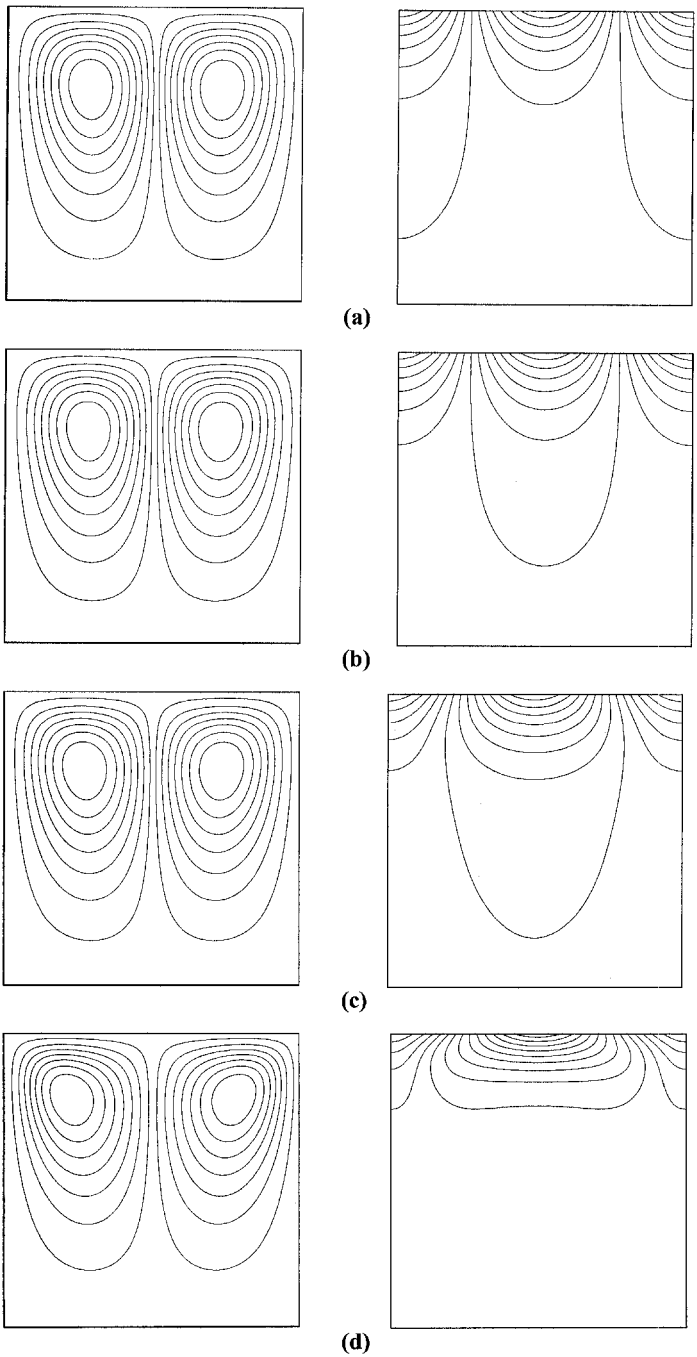

Figure 4. Calculated streamlines and isotherms for (*a*) $\mathrm{Ra} = 10^2$ ($\Psi_{\max} = 8.736 \times 10^{-3}$), (*b*) $\mathrm{Ra} = 10^3$ (8.663×10^{-2}), (*c*) $\mathrm{Ra} = 10^4$ (7.439×10^{-1}), and (*d*) $\mathrm{Ra} = 10^5$ (2.986).

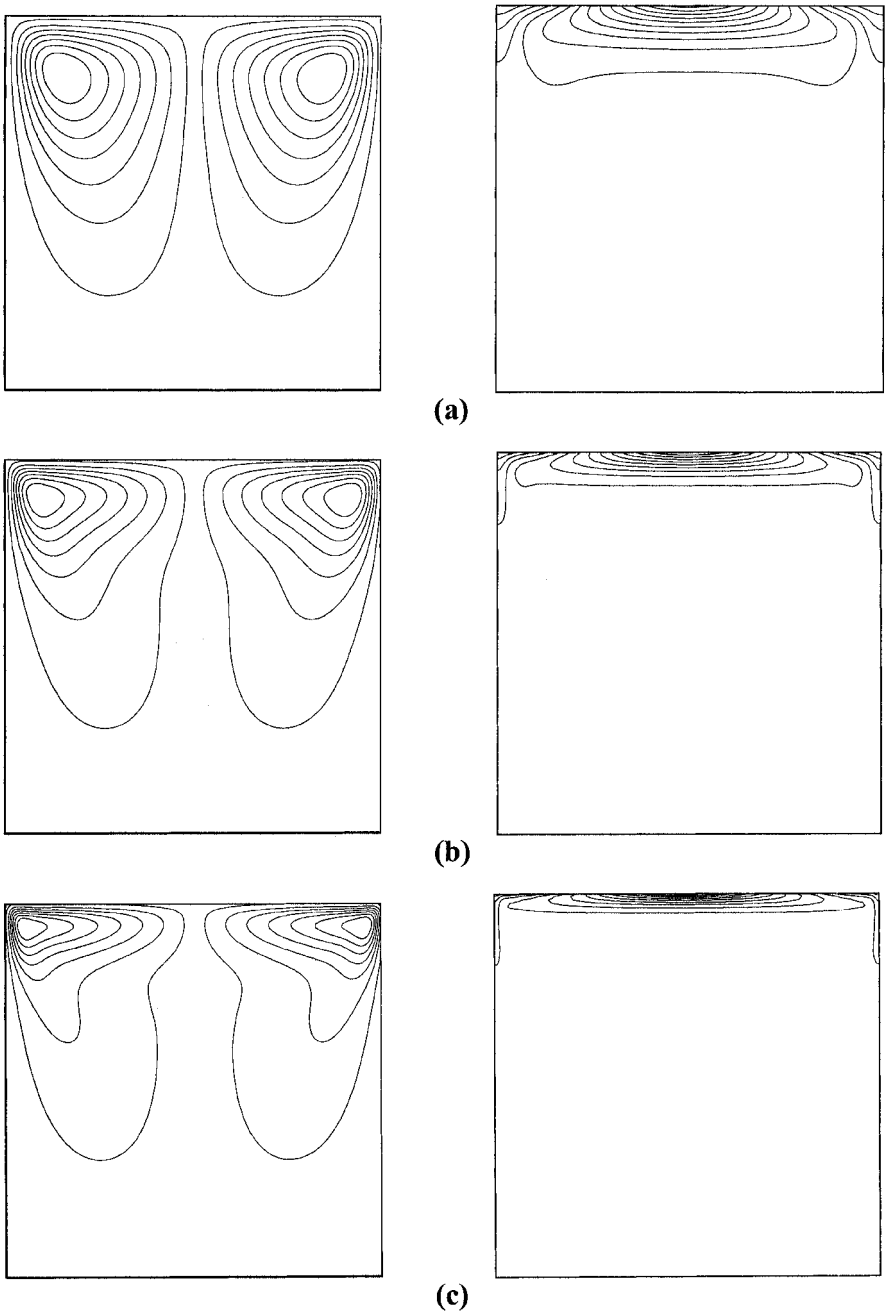

Figure 5. Calculated streamlines and isotherms for (*a*) $Ra = 10^6$ ($\Psi_{max} = 6.997$), (*b*) $Ra = 10^7$ (13.160), and (*c*) $Ra = 10^8$ (22.882).

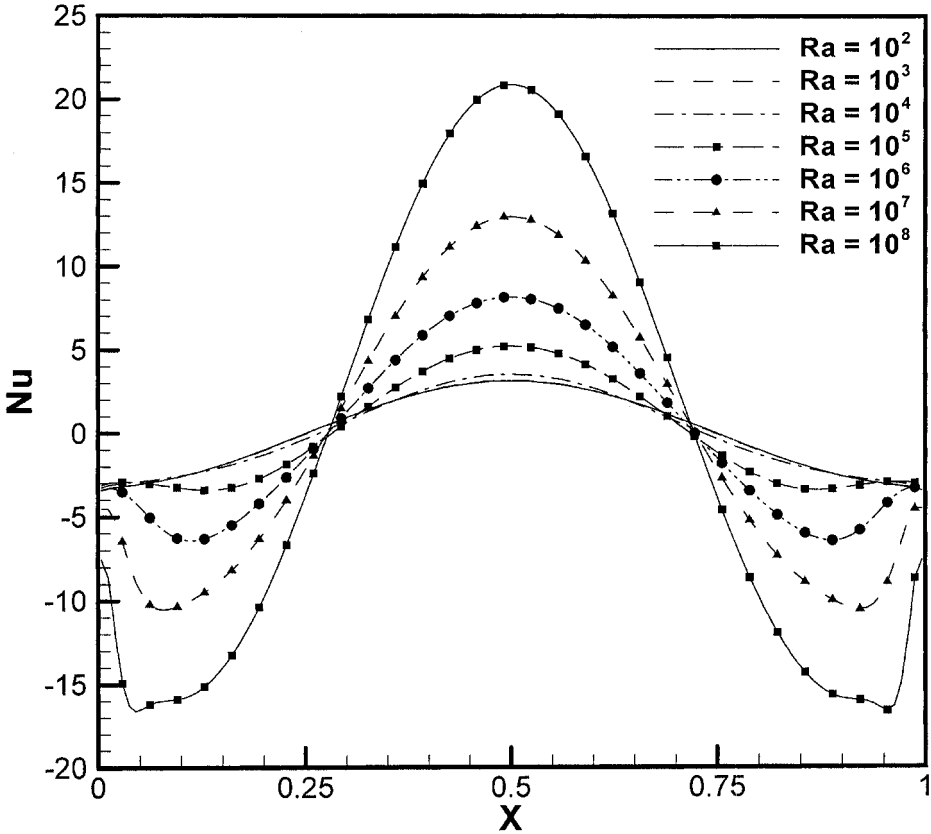

Figure 6. Variation of local Nu on the upper wall with Rayleigh number.

$$\left.\begin{aligned} U = V = 0 \\ \tfrac{\partial \Theta}{\partial Y} = 0 \end{aligned}\right\} \quad \text{for} \quad Y = 0 \text{ and } 0 \le X \le 1 \tag{8b}$$

$$\left.\begin{aligned} U = V = 0 \\ \Theta = \tfrac{1}{2}(1 - \cos(2\pi X)) \end{aligned}\right\} \quad \text{for} \quad Y = 1 \text{ and } 0 \le X \le 1 \tag{8c}$$

Because the computational effort required for this problem was not particularly large, the solution domain covered the whole field.

The values of the stream function are calculated assuming $\Psi = 0$ at $Y = 0$, $X = 0$.

The local Nusselt number, $\mathrm{Nu}(X)$, for the heated upper wall is defined by

$$\mathrm{Nu}(X) = \left[-\frac{\partial \Theta}{\partial Y}\right]_{Y=1} \tag{9}$$

The average Nusselt number, $\overline{\mathrm{Nu}}$, in the upper wall can be defined by

$$\overline{\mathrm{Nu}} = \int_0^1 \mathrm{Nu}(X)\,dX \tag{10}$$

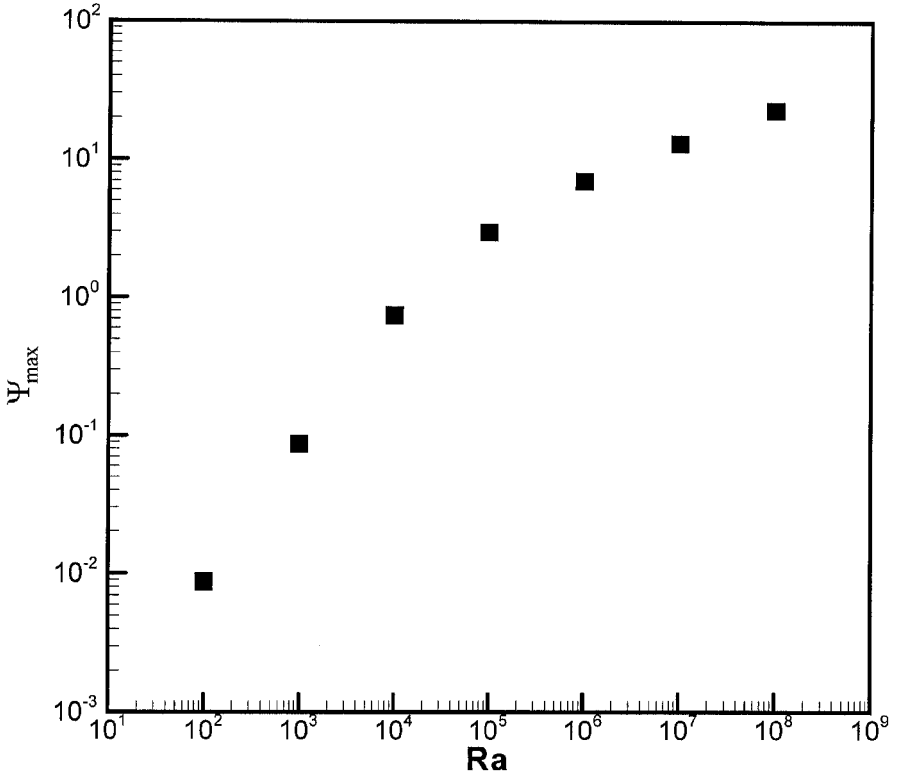

Figure 7. Variation of Ψ_{max} with Rayleigh number.

However, in the present study, the net heat input from the upper wall into the enclosure is zero, and as a consequence the average Nusselt number is also zero.

NUMERICAL PROCEDURE

The above governing equations together with the corresponding boundary conditions are solved numerically, employing a finite-volume method. The semi-implicit method for pressure-linked equations—consistent (SIMPLEC) of van Doormal and Raithby [11] is used to couple momentum and continuity equations in a uniform staggered grid. Uniform grids were selected mainly because they result in smaller discretization errors. In addition there exist gradients in parts of this flow other than only the walls. The momentum equations for U and V and the energy equation are solved using both the power-law scheme of Patankar [12] and the QUICK scheme of Hayase et al. [13] to minimize numerical diffusion. In all calculations presented here, under-relaxation factors with values of 0.9, 0.9, 0.5, and 0.5 were applied to U, V, Θ, and P, respectively.

The iterative procedure is initiated with an arbitrary velocity field followed by the solution of the energy equation and is continued until convergence is achieved.

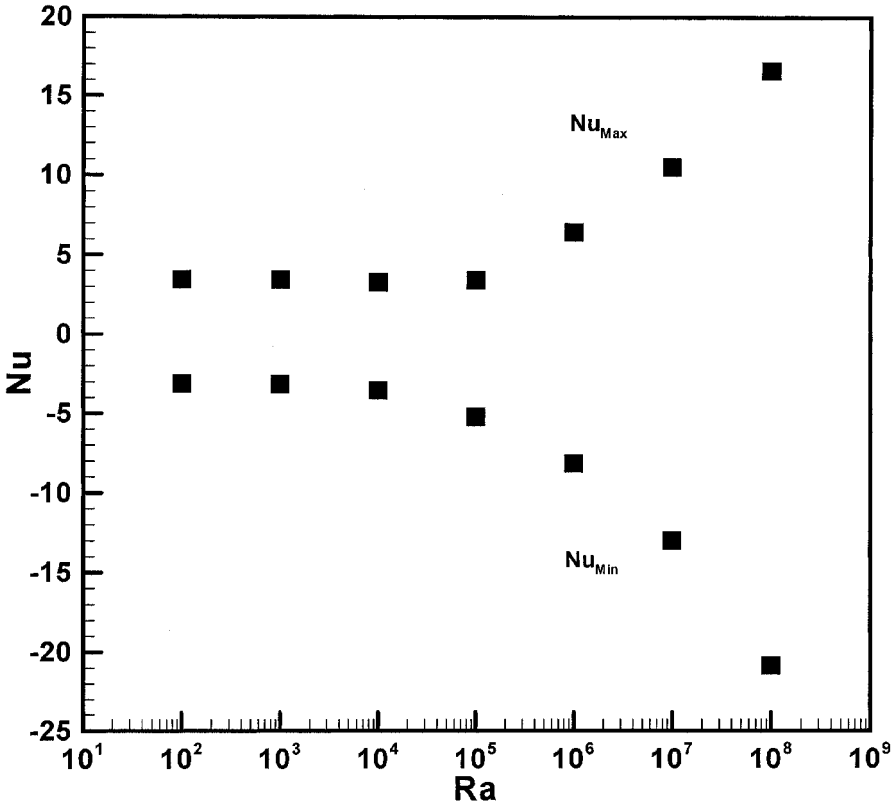

Figure 8. Variation of maximum and minimum values of Nu on the upper wall with Ra.

Convergence is established through the sum of the absolute relative errors for each dependent variable in the entire flow field:

$$\sum_{i,j} \frac{|\varphi_{i,j}^{n+1} - \varphi_{i,j}^{n}|}{|\varphi_{i,j}^{n+1}|} \leq \varepsilon \tag{11}$$

where φ represents the variables U, V, or Θ, the superscript n refers to the iteration number, and the subscripts i and j refer to the space coordinates. The value of ε is chosen as 10^{-5} for all calculations. All calculations are carried out on Intel CPU-based personal computers.

Before the final computations, a grid independence test was performed using successively sized grids, 41×41, 61×61, 81×81, 121×121, 161×161, and 241×241, and three representative Rayleigh numbers 10^5, 10^6, and 10^8. The variation of the maximum value of the stream function, Ψ_{max}, with the grid size appears to be negligible for grid sizes larger than 121×121, as shown in Figure 2. The grid size also influences the maximum and minimum values of the local Nusselt number, Nu, at the upper heated wall, as shown in Figure 3. This influence is most significant for the highest Rayleigh number of $Ra = 10^8$. When the mesh is refined from 121×121 to

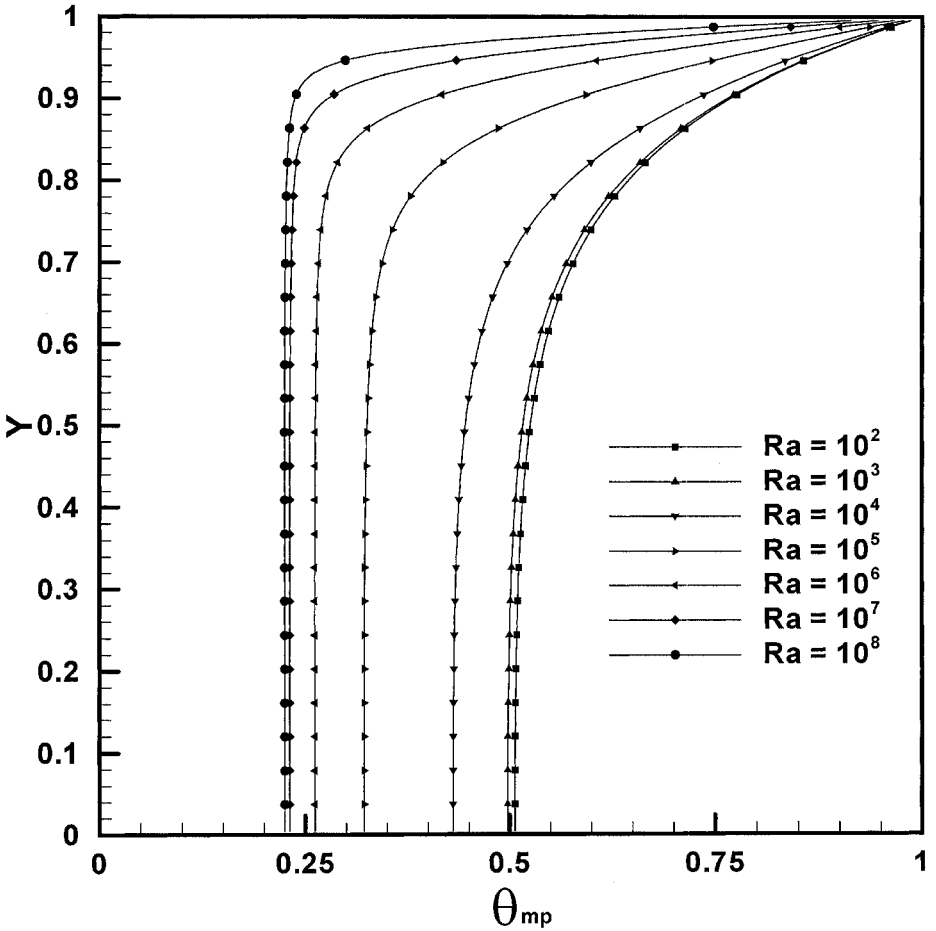

Figure 9. Temperature distribution in the middle plane of the enclosure.

161×161 grid points the local Nusselt number decreases by less than 1%, whereas for $Ra = 10^6$ it decreases by less than 0.5% and for $Ra = 10^5$ by less than 0.4%. The small changes in Ψ_{max} and Nu described above suggest that a grid size of 121×121 is adequate for engineering calculations to resolve the corresponding velocity and temperature fields.

The present computational fluid dynamics (CFD) source code was validated against the numerical results of Ganzarolli and Milanez [14] for natural convection in a cubical enclosure heated from below and cooled symmetrically from the sidewalls. It was also validated against the benchmark numerical solution of de Vahl Davis [15] for natural convection of air in a square cavity. In the first test case, a working fluid of Pr equal to 7.0 was used with Rayleigh numbers ranging from 10^3 to 10^7. A uniform grid of 61×61 was used. The comparison was based on the maximum value of the stream function Ψ_{max} and the Nu for the specified range of Rayleigh numbers. The observed differences with respect to the average Nu are approximately 0.2%, and with respect to the value of Ψ_{max} are about 0.05%. In the second test case of de Vahl

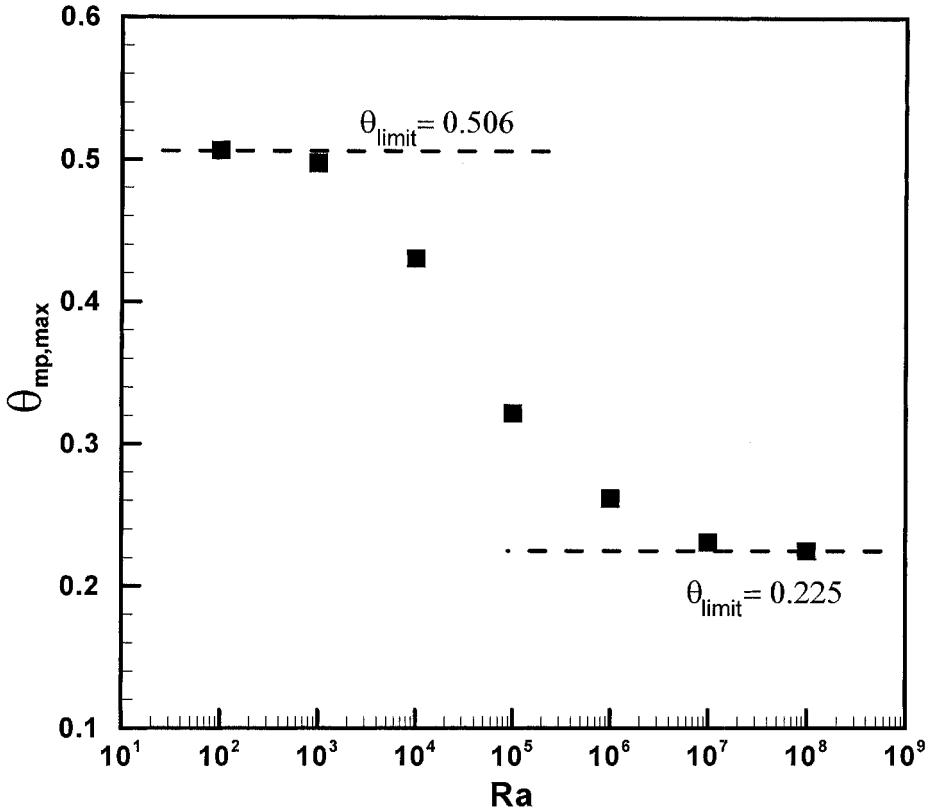

Figure 10. Variation of the asymptotic temperature with Ra.

Davis [15], comparisons were made for a range of Rayleigh numbers, using the same uniform grid. These comparisons were based on the maximum value of the field velocity and its position, the maximum value of the stream function and its position, the average, and local Nusselt number. The observed differences between the present results and those of de Vahl Davis [15] for all variables and cases examined was less than 0.05%. The values of the average and local Nusselt number were found to be more sensitive to the grid size with increasing Rayleigh numbers.

RESULTS AND DISCUSSION

A parametric study was carried out to determine the influence of Rayleigh number on the flow field of a high Pr ($=100$) fluid. Lim et al. [16] showed that there is only a minor influence of Prandtl number on the natural convection in glass-melting furnaces for $Pr \gg 1$. A range of Rayleigh numbers from 10^2 to 10^8 was considered that covers the whole range encountered in glass tanks. The influence of the enclosure aspect ratio was also examined for the values of 0.5, 1.0, and 2.0.

The main characteristics of natural convection in the present enclosure with the upper wall subjected to a sinusoidal temperature distribution are shown in Figures 4 to 7. The flow and temperature fields are presented in terms of streamlines and

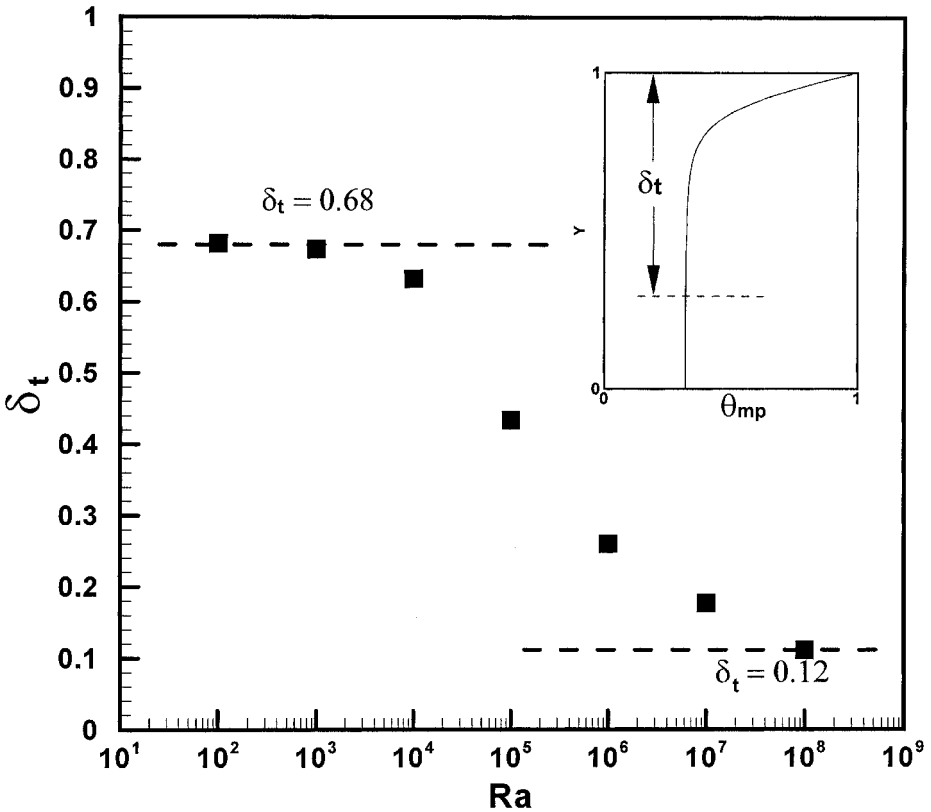

Figure 11. Variation of thermal boundary layer thickness in the middle plane with Ra.

isotherms, with 15 equally spaced contour levels drawn in all cases. These figures show that, due to the symmetric boundary condition at the upper wall together with the adiabatic conditions on the side and bottom walls, both the flow and temperature fields are symmetric about the midplane of the enclosure. A pair of identical counter-rotating cells is formed in the left and right halves of the enclosure. The fluid moves horizontally from the hotter middle of the upper wall toward its colder edge; then it descends along the adiabatic cooler sidewall; and finally it ascends near the symmetry plane.

Figure 4 shows the streamlines and the isotherm contours obtained for $Ra = 10^2$, 10^3, 10^4, and 10^5, and Figure 5 for the higher Rayleigh numbers of 10^6, 10^7, and 10^8. In the range of Rayleigh numbers 10^2 to 10^4, the circulation patterns in the enclosure are very weak because the viscous forces are dominating over the buoyant forces. The temperature fronts penetrate from the upper wall deep inside the fluid body, as conduction is the main heat transfer mechanism in this case. With increasing Rayleigh number, the intensity of the recirculation patterns increases and the centers of the cells move upward. At approximately $Ra = 10^5$, the isotherms start to concentrate near the upper wall, indicating that the advection mode of the heat transfer begins to dominate over conduction. Beginning with $Ra = 10^6$, we see that

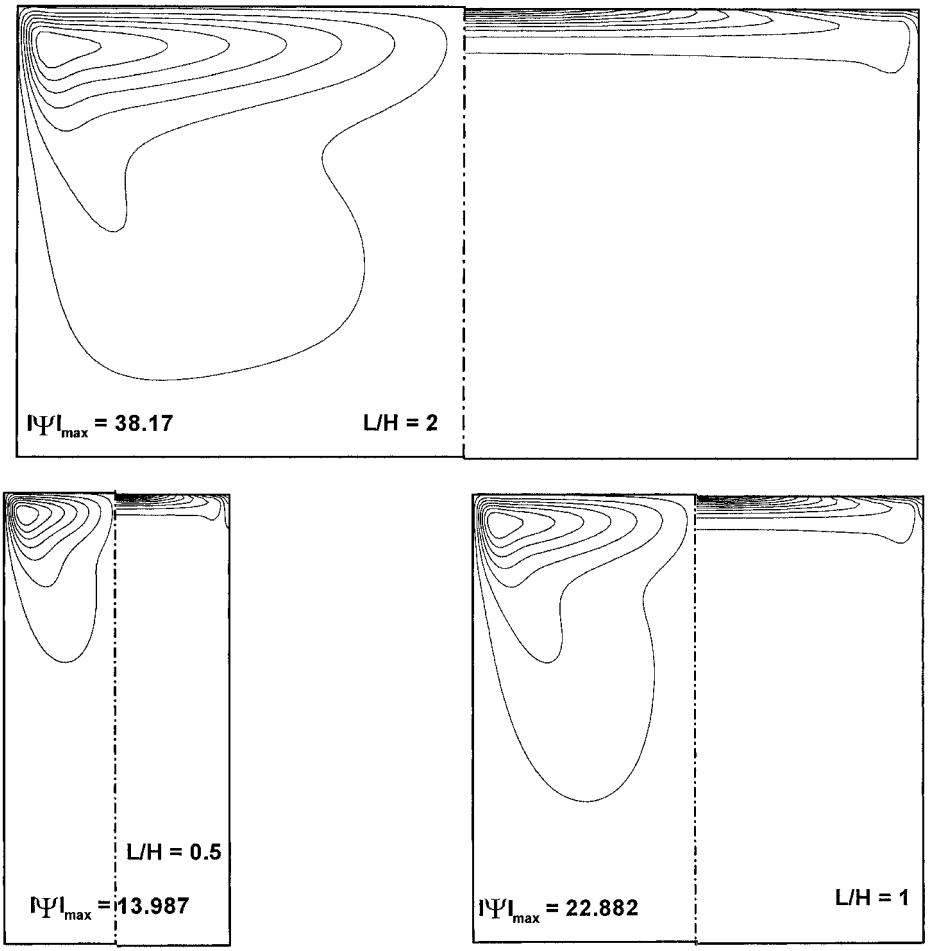

Figure 12. Streamlines and isotherms for Ra $= 10^8$ and aspect ratios of 0.5, 1.0, and 2.0.

the temperature gradients are confined to the upper wall in the form of a thermal boundary layer. This zone becomes thinner with increasing Rayleigh number. The centers of the recirculation zones move toward the corners of the upper wall of the enclosure, and at the higher Rayleigh numbers of 10^7 and 10^8, they are confined in the corners. In these last two cases, it appears that there is no significant heat transfer to the main fluid body. The confinement of the flow in the upper wall corners of the enclosure causes an increased heat transfer there.

Owing to the symmetry in the temperature field, the heat transfer is also symmetrical with respect to the midplane ($X = 0.5$). Figure 6 shows the variation of local Nusselt number along the upper wall for the Rayleigh numbers studied. The higher the Ra number, the larger the amount of heat added to the fluid in the central region of the enclosure, which in turn intensifies fluid convection. In the middle region of the top wall the cold fluid that is brought there by the recirculation patterns

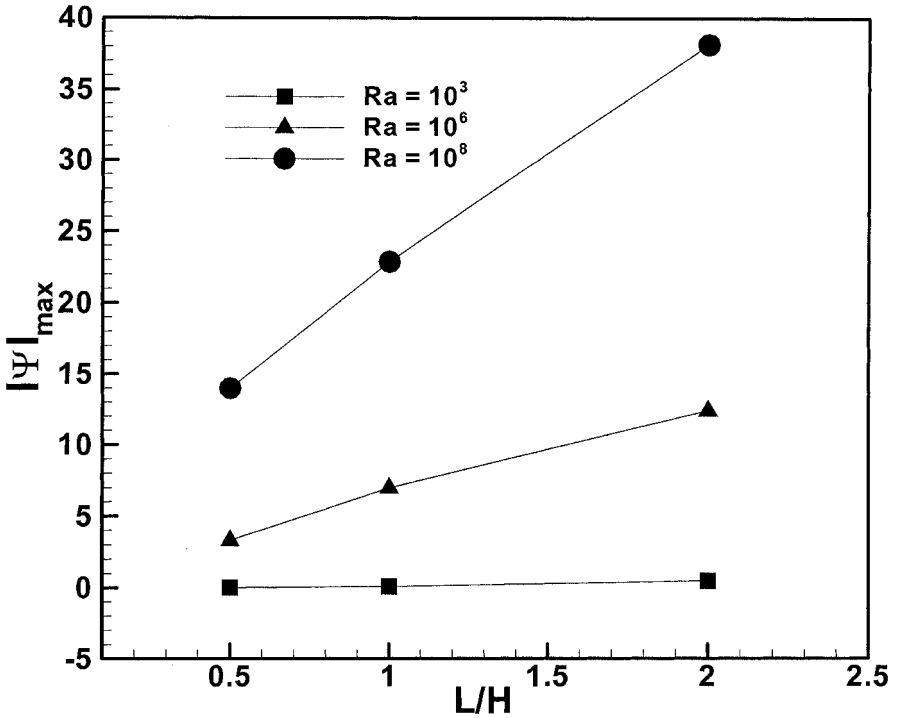

Figure 13. Variation of Ψ_{max} with aspect ratio for Ra $= 10^3$, 10^6, and 10^8.

from the lower part of the enclosure is heated up and as a result the local Nusselt number becomes positive there. The heated fluid from the middle of the upper wall reaches the enclosure corners, losing heat to the upper wall, and thus the local Nusselt number becomes negative there. For the higher Rayleigh numbers, the recirculation centers become very close to the upper wall while the recirculation intensity increases, producing two symmetric peaks in the Nusselt number near the top corners of the enclosure.

The effect of Rayleigh number on the intensification of the fluid circulation is evident in Figure 7, where an increase of Rayleigh number causes an analogous increase of the Ψ_{max} value.

The variation of the maximum and minimum values of the local Nusselt number as a function of Ra is shown in Figure 8. The heat transfer rates show a large increase for Rayleigh number values higher than 10^6. In contrast, for Ra less than 10^5 the heat transfer rates remain practically the same.

The temperature distribution in the middle plane of the enclosure, shown in Figure 9, is quite helpful in assessing the penetration depth of the temperature boundary layer formed on the top wall of the enclosure. In particular, for every Rayleigh number studied, the dimensionless temperature takes the value of 1 at the top of the middle plane of the enclosure and then decreases with increasing distances from the upper wall. Conduction and convection are the two antagonistic mech-

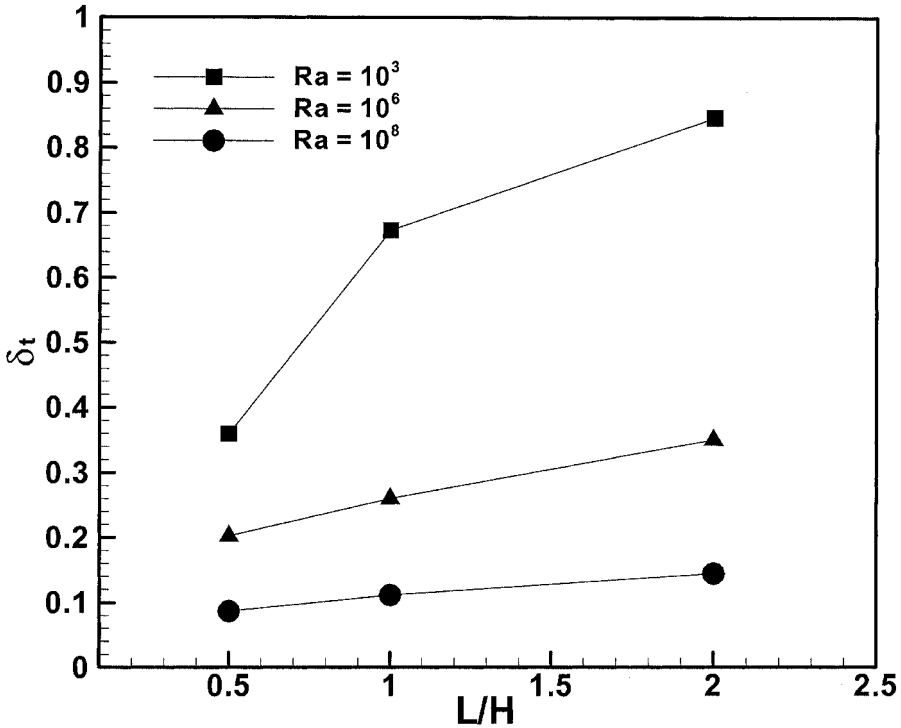

Figure 14. Variation of thermal boundary layer thickness in the middle plane with aspect ratio for $Ra = 10^3$, 10^6, and 10^8.

anisms depending on the specific value of Rayleigh number. In the case of the lower Rayleigh number of 10^2, the middle-plane temperature Θ_{mp} reaches an asymptotic value in the core region of the enclosure that corresponds to the heat transfer by pure conduction. The increase in the Ra number causes a decrease in the asymptotic value of the middle-plane temperature in the core region, as a consequence of the dominance of convective heat transfer. In this last case, the thermal boundary layer becomes thinner, indicating that the heat transfer takes place in the region near the upper wall without much penetration into the main fluid body.

The distribution of the asymptotic value of the middle-plane temperature in the core region of the enclosure for all Rayleigh numbers studied is shown in Figure 10. This value corresponds to the maximum possible temperature at the bottom wall and varies between a lower-limit value of approximately 0.22 and a higher-limit value of approximately 0.50. The temperatures at the bottom wall corners have significantly lower values and may cause solidification of the glass melt, a fact that should be considered in the design of glass furnaces.

The thickness of the thermal boundary layer based on the temperature distribution in the middle plane of the enclosure is shown in Figure 11 for all Rayleigh numbers studied. This thickness reaches an approximate upper limit of $\delta_t = 0.68$ for the lower Rayleigh number value and an approximate lower limit of $\delta_t = 0.12$ for the higher Rayleigh number value.

The influence of the aspect ratio on the established flow and temperature fields in the enclosure is shown in Figure 12 where the streamlines (left side) and the isotherms (right side) are presented for values of aspect ratio $L/H = 0.5$, 1.0, and 2.0 and for Ra value of 10^8. The increase of the aspect ratio results in a circulation pattern covering a larger area of the enclosure. It appears that the centers of the circulating fluid move closer and the flow is confined to the upper top wall for the lower aspect ratio value of 0.5. Figure 13 shows the variation of Ψ_{max} with aspect ratio for Ra values of 10^3, 10^6, and 10^8, which represents a combined measure of intensity and extent of the recirculation region. It is shown that the value of Ψ_{max} increases with increasing aspect ratio and Rayleigh number. Thus, a larger mass of glass melt is circulated and homogenized, which implies improvement in glass production. Figure 14 presents the corresponding variation of the thermal boundary layer thickness δ_t at the enclosure middle plane. The thermal penetration into the fluid body becomes larger with increasing aspect ratio. The influence of the aspect ratio on the thermal penetration depth is quite large mainly for the lower Rayleigh number of $Ra = 10^3$, whereas for $Ra = 10^8$, it becomes almost insignificant. The optimum conditions for glass production are intense recirculation patterns combined with large thermal penetration depths. This can be achieved employing large Rayleigh numbers combined with large tank aspect ratios.

CONCLUSIONS

In this investigation, numerical results of natural convection heat transfer in a two-dimensional enclosure subjected to steady sinusoidal temperature boundary condition on the upper wall with adiabatic bottom and sidewalls are presented. The influence of Rayleigh number on the flow patterns and heat transfer characteristics in the enclosure is examined in detail for a large range of Rayleigh numbers. The flow and temperature fields are symmetric about the middle plane of the enclosure due to the imposed symmetry condition on the upper wall boundary. From the results presented above, the following main conclusions may be drawn.

1. For small Ra, the heat transfer is dominated by conduction across the fluid layers.
2. The process begins to be dominated by convection with increasing Ra, and at very high Rayleigh numbers the effect of conduction diminishes.
3. The recirculation patterns move apart and toward the corresponding upper wall corners with increasing Rayleigh number.
4. A thermal boundary layer is formed on the upper wall with its thickness decreasing as the Rayleigh increases. This results in a lower temperature penetration depth and may have important implications in the design of glass melting tanks.
5. Finally, increasing the tank aspect ratio increases the fluid circulation intensity and the thermal penetration depth, which are important parameters for improving glass melt homogenization. Optimum conditions for glass production can be achieved employing large Rayleigh numbers combined with large tank aspect ratios.

REFERENCES

1. I. E. Sarris, N. Katsavos, I. Lekakis, and N. S. Vlachos, Modelling the Influence of Combustion on Glass Melt Flow (in Greek), in *Proc. 6th National Conf. of Solar Technology Institute*, Greece, vol. 2, pp. 201–209, University of Thessaly, Volos, 1999.
2. C. Q Jian, A. Dutta, A. Mukhopadhyay, and D. P. Tselepidakis, Explicit Coupling Between Combustion Space and Glass Tank Simulations for Complete Furnace Analysis, in *Proc. 1st Balkan Conf. on Glass Science and Technology*, Greece, pp. 402–409, University of Thessaly, Volos, 2000.
3. S. Ostrach, Natural Convection in Enclosures, *Advances in Heat Transfer*, vol. 8, pp. 161–227, 1972.
4. O. Aydin, A. Unal, and T. Ayhan, Natural Convection in Rectangular Enclosures Heated from One Side and Cooled from the Ceiling, *Int. J. Heat Mass Transfer*, vol. 42, pp. 2345–2355, 1999.
5. D. Poulikakos, Natural Convection in a Confined Fluid-Filled Space Driven by a Single Vertical Wall with Warm and Cold Regions, *ASME J. Heat Transfer*, vol. 107, pp. 867–876, 1985.
6. E. Bilgen, X. Wang, P. Vasseur, F. Meng, and L. Rabillard, On the Periodic Conditions to Simulate Mixed Convection Heat Transfer in Horizontal Channels, *Numerical Heat Transfer, Part A*, vol. 27, pp. 461–472, 1995.
7. E. K. Lakhal, M. Hasnaoui, P. Vasseur, and E. Bilgen, Natural Convection in a Square Enclosure Heated Periodically from Part of the Bottom Wall, *Numerical Heat Transfer, Part A*, vol. 27, pp. 319–333, 1995.
8. J. I. Lage and A. Bejan, The Resonance of Natural Convection in an Enclosure Heated Periodically from the Side, *Int. J. Heat and Mass Transfer*, vol. 36, pp. 2027–2038, 1993.
9. S. Wright and H. Rawson, Calculation of Natural Convection in a Rectangular Cell Containing Glass with Specified Temperatures on the Boundaries, *Glass Technology*, vol. 14, pp. 42–49, 1973.
10. D. M. Burley, A. Moult, and H. Rawson, Application of the Finite Element Method to Calculate Flow Patterns in Glass Tank Furnaces, *Glass Technology*, vol. 19, pp. 86–91, 1978.
11. J. P. Van Doormal and G. D. Raithby, Enhancements of the SIMPLE Method for Predicting Incompressible Fluid Flows, *Numerical Heat Transfer*, vol. 7, pp. 146–163, 1984.
12. S. V. Patankar, *Numerical Heat Transfer and Fluid Flow*, Hemisphere, London, 1980.
13. T. Hayase, J. A. C. Humphrey, and R. Greif, A Consistently Formulated QUICK Scheme for Fast and Stable Convergence Using Finite-Volume Iterative Calculation Procedure, *J. Comput. Physics*, vol. 98, pp. 108–118, 1992.
14. M. M. Ganzarolli and L. F. Milanez, Natural Convection in Rectangular Enclosures Heated from Below and Symmetrically Cooled from the Sides, *Int. J. Heat Mass Transfer*, vol. 38, pp. 1063–1073, 1995.
15. G. de Vahl Davis, Natural Convection of Air in a Square Cavity: A Bench Mark Numerical Solution, *Int. J. Num. Methods Fluids*, vol. 3, pp. 249–264, 1983.
16. K. O. Lim, T. H. Song, K. S. Lee, Patterns of Natural Convection Driven by the Free Surface Temperature Distribution in a Glass Melting Furnace, *Glass Technology*, vol. 38, pp. 27–31, 1998.